

ADVANCED MATERIALS

Supporting Information

for *Adv. Mater.*, DOI: 10.1002/adma.201600160

Giant Resistive Switching via Control of Ferroelectric Charged Domain Walls

*Linze Li, Jason Britson, Jacob R. Jokisaari, Yi Zhang,
Carolina Adamo, Alexander Melville, Darrell G. Schlom,
Long-Qing Chen, and Xiaoqing Pan**

Supporting Information

Giant resistive switching *via* control of ferroelectric charged domain walls

*Linze Li, Jason Britson, Jacob R. Jokisaari, Yi Zhang, Carolina Adamo, Alexander Melville, Darrell G. Schlom, Long-Qing Chen, and Xiaoqing Pan**

Phase-field simulations: BiFeO₃ thin-film domain structures were simulated using the phase field approach that has been described extensively in previous publications^[37-39]. Domain structures were modeled as continuous distributions of the three polar components, P_i , while the antiferromagnetic behavior of BiFeO₃ was neglected^[40] [ENREF 38](#). Starting from an initial polarization distribution to describe an experimentally observed domain structure, the polarization components were evolved toward a local minimum in the total system free energy, F , by solving the time dependent Ginzburg-Landau equation

$$\frac{\partial P_i}{\partial t} = -L \frac{\delta F}{\delta P_i}. \quad (1)$$

In equation 1 L is a constant related to the domain wall mobility that is taken to have a value of one in the simulations. Here, total free energy consisted of contributions from the bulk free energy of BiFeO₃, electrostatic energy of interactions between polarization bound charges, mechanical energy from long range elastic interactions and gradient energy associated with domain walls. The bulk free energy of BiFeO₃ was described by a fourth-order Landau polynomial with respect to the polarization

$$f_{bulk} = \alpha_1 (P_1^2 + P_2^2 + P_3^2) + \alpha_{11} (P_1^4 + P_2^4 + P_3^4) + \alpha_{12} (P_1^2 P_2^2 + P_2^2 P_3^2 + P_3^2 P_1^2) \quad (2)$$

for the stress-free bulk material utilizing phenomenological constants from prior publications^[37, 40, 41] [ENREF 37](#) [ENREF 38](#). These coefficients, in SI units, were

$\alpha_1 = 4.9(T - 1103) \times 10^8$, $\alpha_{11} = 6.50 \times 10^8$, and $\alpha_{12} = 1.0 \times 10^8$ [37]. The simulation used room temperature of $T = 298$ K.

Electrostatic and mechanical energy were included through long-range electric and elastic stress fields in the system. Expressions for these contributions to the energy are described in previous publications [39, 42]. The distribution of the electric potential in the system was found for a given polarization distribution by solving the Poisson equation using the background dielectric constant [43] assumed to be 10. This portion of the dielectric constant does not include the changes in electrical displacement due to the polarization, which was included explicitly in the model. Only polarization bound charge was considered in the model and any free charges were neglected in the calculation of the electrical energy. For the solution to the Poisson equation we assumed ideally compensating electrodes that fixed the potential at the top and bottom film surfaces and were both assumed to be grounded. These electrodes were specified through the boundary condition on the Poisson equation as explained in previous publications [42].

Stress and strain fields associated with spontaneous strains in the film due to the ferroelectric transition [44] were found by solving the equations for mechanical equilibrium, $\sigma_{ij,j} = 0$, with boundary conditions appropriate to thin films as described in previous publications [38, 45]. For this simulation the electrostrictive constants in Voigt notation, Q_{ij} , leading to the spontaneous strain from the cubic parent phase were $Q_{11} = 0.032 \text{ C}^{-2} \text{ m}^4$, $Q_{12} = -0.016 \text{ C}^{-2} \text{ m}^4$ and $Q_{44} = 0.02 \text{ C}^{-2} \text{ m}^4$. Similarly, the elastic constants used in the model were $C_{11} = 300$ GPa, $C_{12} = 162$ GPa and $C_{44} = 69.1$ GPa [37]. These constants reflect the symmetry of the parent paraelectric phase [45].

The domain wall energy was incorporated into the model by adding an energy associated with gradients in the polarization. For simplicity, an isotropic domain wall energy was modeled with the expression

$$f_{DW} = \frac{1}{2} G P_{ij}^2, \quad (3)$$

where G is the gradient energy coefficient that is related to the Landau coefficients and characteristic system length^[38] of 1.0 nm. Throughout this manuscript this constant was assumed to have a value of $1.1 \times 10^{-10} \text{ C}^{-2} \text{ m}^4 \text{ N}$, which resulted in estimated domain wall energies in the model of about 110 mJ m^{-2} , 260 mJ m^{-2} , and 70 mJ m^{-2} for non-charged 71° , 109° , and 180° domain walls, respectively. These results are in reasonably good agreement with previous theoretical estimations based on density functional theory that have estimated the 71° , 109° and 180° domain wall energies ranging between 128 and 360 mJ m^{-2} , 33 and 205 mJ m^{-2} , and 98 and 829 mJ m^{-2} for the 71° , 109° and 180° domain wall energies, respectively^[46-48].

The thin film was simulated on a quasi-two dimensional grid of $256\Delta \times 1\Delta \times 80\Delta$ where the grid spacing, Δ , was assumed to be 0.5 nm. Periodic boundary conditions were assumed in the first two dimensions, while non-periodic boundary conditions described above were assumed along the third, out-of plane dimension. A film thickness of 20 nm was used, with a 10 nm thick layer of substrate allowed to relax beneath the bottom of the film^[38]. The remaining points were included as padding for numerical stability. In the $\text{TbScO}_3/\text{BiFeO}_3$ system lattice matching between the substrate and thin film results in only a small biaxial strain^[33] and the phase field model reflected this by assuming that the biaxial coherency strain imposed by the substrate was 0.0%. This led to a system in which the substrate constrained the overlying thin film, but did not apply a compressive biaxial strain that may have led to a transition to the tetragonal phase in the thin film. The solution to the model was found by iteratively solving equation 1, where the temporal derivative was approximated with a finite difference with a time step of $t/t_0 = 0.01$.

- [37] B. Winchester, P. Wu, L. Q. Chen, *Appl. Phys. Lett.* **2011**, *99*, 052903.
- [38] Y. L. Li, S. Y. Hu, Z. K. Liu, L. Q. Chen, *Acta Mater.* **2002**, *50*, 395.
- [39] H. L. Hu, L. Q. Chen, *J. Am. Ceram. Soc* **1998**, *81*, 492.
- [40] J. X. Zhang, Y. L. Li, Y. Wang, Z. K. Liu, L. Q. Chen, Y. H. Chu, F. Zavaliche, R. Ramesh, *J. Appl. Phys.* **2007**, *101*, 114105.
- [41] J. X. Zhang, R. Wu, S. Choudhury, Y. L. Li, S. Y. Hu, L. Q. Chen, *Appl. Phys. Lett.* **2008**, *92*, 122906.
- [42] Y. L. Li, S. Y. Hu, Z. K. Liu, L. Q. Chen, *Appl. Phys. Lett.* **2002**, *81*, 427.
- [43] A. Tagantsev, *Ferroelectrics* **1986**, *69*, 321.
- [44] A. F. Devonshire, *Philos Mag* **1949**, *40*, 1040.
- [45] L. Q. Chen, *J. Am. Ceram. Soc* **2008**, *91*, 1835.
- [46] J. X. Zhang, X. X. Ke, G. Y. Gou, J. Seidel, B. Xiang, P. Yu, W. I. Liang, A. M. Minor, Y. H. Chu, G. Van Tendeloo, X. B. Ren, R. Ramesh, *Nat. Commun.* **2013**, *4*.
- [47] Y. B. Chen, M. B. Katz, X. Q. Pan, R. R. Das, D. M. Kim, S. H. Baek, C. B. Eom, *Appl. Phys. Lett.* **2007**, *90*, 072907.
- [48] A. Lubk, S. Gemming, N. A. Spaldin, *Phys. Rev. B* **2009**, *80*, 104110.

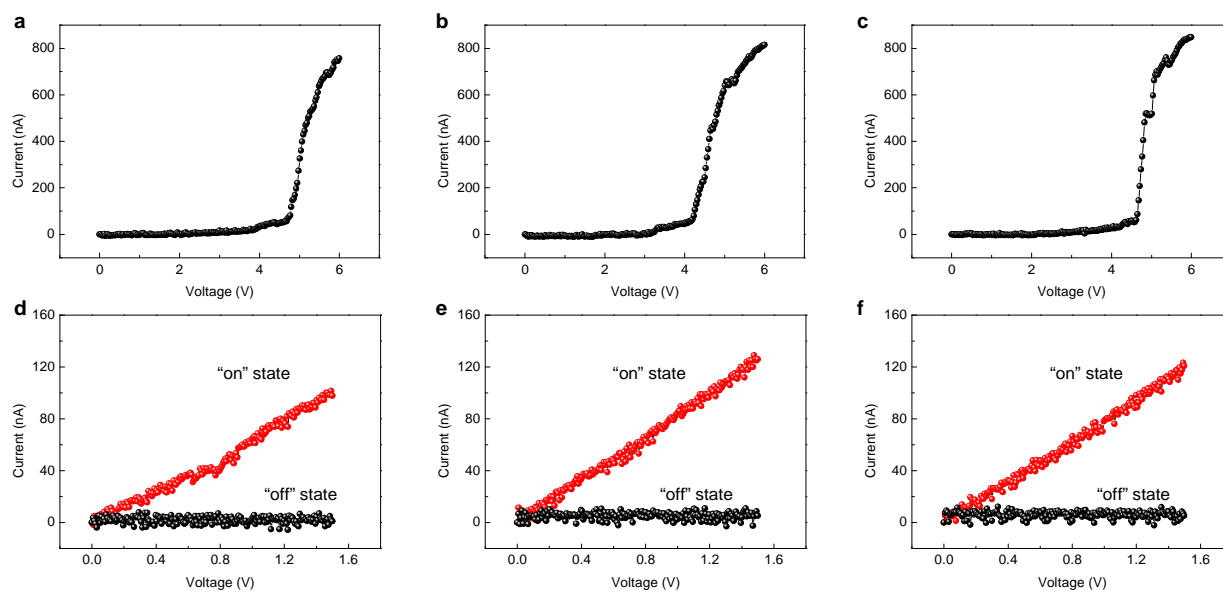


Figure S1. Repeatability of the sCDW assisted resistive switching. **a-c**, Three repetitive I-V curves showing the resistive switching measured in *in situ* TEM, at different spots of the same BiFeO₃ thin film where the same type of sCDW exists. **d-f**, Three repetitive *in situ* measured readout current of the system with (“on” state) and without (“off” state) a sCDW at different spots of the same BiFeO₃ thin film.

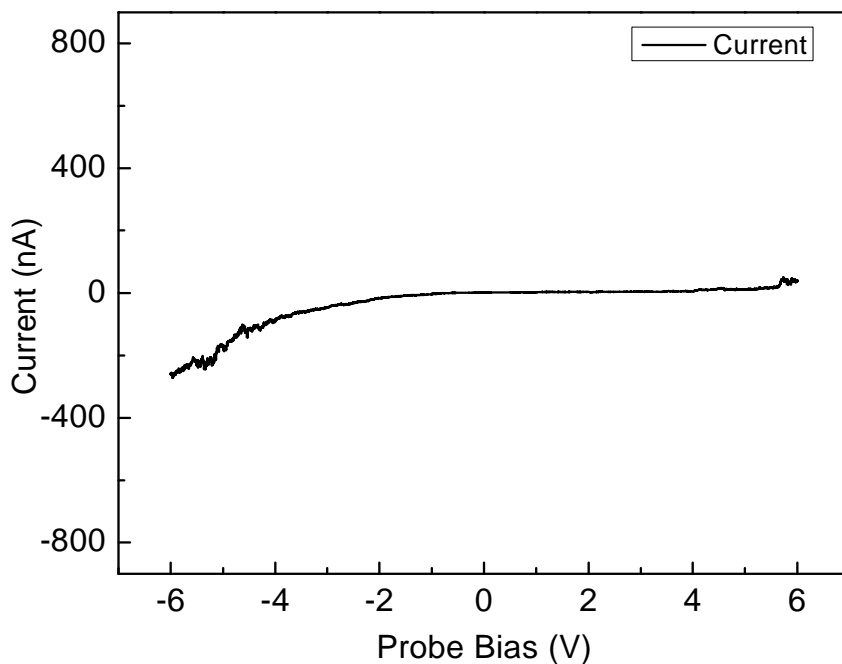


Figure S2. Current versus voltage curves taken in situ by applying a bias between the tungsten surface probe and the buffer $\text{La}_{0.7}\text{Sr}_{0.3}\text{MnO}_3$ electrode in a region that is originally monodomain. For the positive branch, the polarization switching occurred at $V = \sim 2.0$ V. This switching did not cause any detectable current change. Since the currents for the voltage range from 0 to 6.0 V remained low, the dramatically increased current observed in Fig. 2h is likely caused by the sCDW.

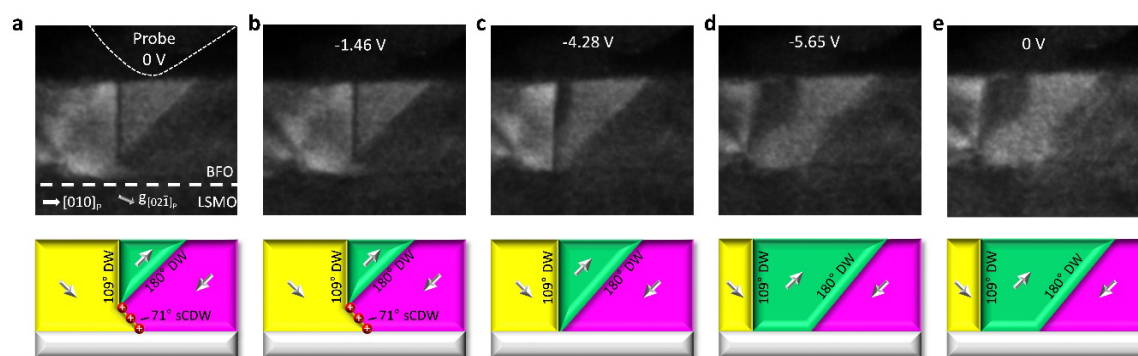


Figure S3. Erasure of a sCDW caused by a negative ramp bias. **a**, The original stable state with a sCDW. **b**, At the critical bias, the domain wall started to move. **c**, The sCDW was annihilated as a result of the expansion of the triangular domain. **d**, The system went back to the stable state without a sCDW. **e**, After removal of the bias, this state remained stable. For scale, the film thickness is 20 nm.

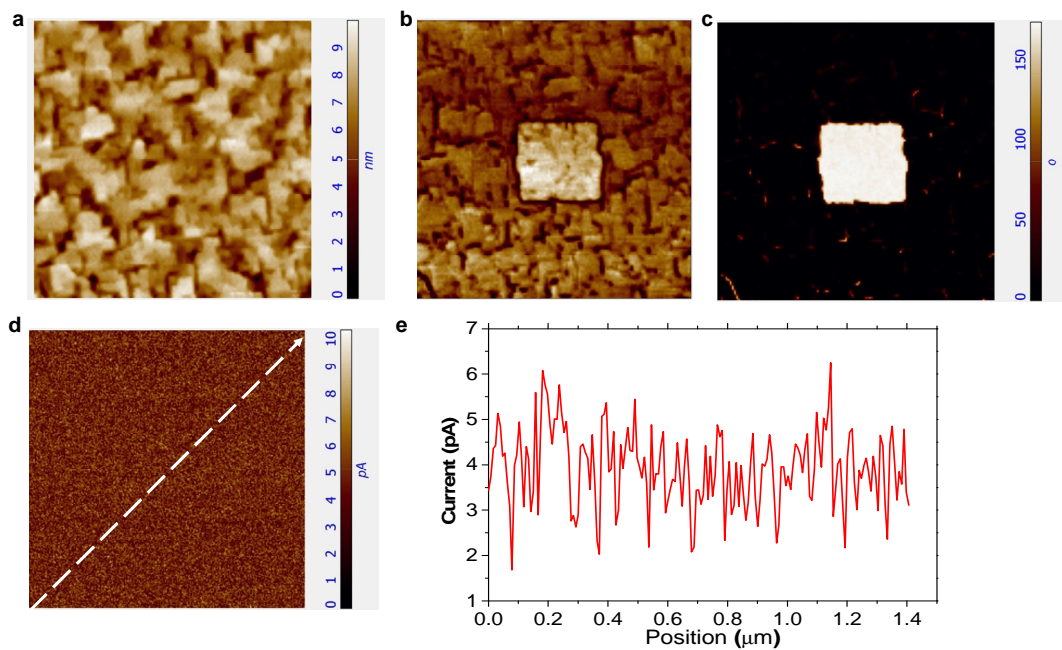


Figure S4. Conductivity of bulk domains and uncharged domain walls in the BiFeO_3 thin film. **a**, Topography, **b**, PFM amplitude and **c**, phase images of a square domain written with a tip bias of -5 V. **d**, SSRM measurement at 1.5 V tip bias, showing that the current through bulk domains and uncharged domain walls is lower than several picoamperes. **e**, Line profiles of SSRM current over the dashed line in **d**. For scale, the size of the scanned region is $1\mu\text{m}\times 1\mu\text{m}$.